Available online www.jocpr.com

Journal of Chemical and Pharmaceutical Research, 2015, 7(4):1254-1273

Research Article

ISSN : 0975-7384
CODEN(USA) : JCPRC5

Synthesis, crystal structure, spectral analysis and theoretical investigation of (E)-3-(4-(dimethylamino)phenyl)-1-(2-hydroxyphenyl)prop-2-en-1-one by DFT and AIM theory

Ashok Kumar Singh* and Ravindra Kumar Singh

Department of Chemistry, Faculty of Science, University of Lucknow, Lucknow, U.P. India

---

ABSTRACT

A new chalcone (E)-3-(4-(dimethylamino) phenyl)-1-(2-hydroxyphenyl) prop-2-en-1-one was synthesized and characterized by elemental analyses, FT-IR, ^{1}H NMR, UV-Vis spectroscopy and single crystal X-ray. Quantum chemical calculations have been performed at DFT level of theory using B3LYP functional and 6-311G (d, p) as basis set. The geometrical parameters of the compound obtained from XRD studies are in agreement with the calculated DFT parameters. The calculated ^{1}H NMR chemical shifts using gauge including atomic orbitals (GIAO) approach are in good conformity with the observed chemical shifts. Potential energy distribution (PED) for the normal modes of vibrations was done using Gar2ped program. The time dependent density functional theory (TD-DFT) was used to assign the nature of different electronic transitions within molecule in gas as well as in solvent phase. Non linear optical (NLO) behavior of title compound was investigated by the computed value of first hyperpolarizability (β_0). Also, the solvent induced effect on the NLO properties were studied by using self-constitent reaction field (SCRF) method using polarised continuum model (PCM). Stability of molecules as a result of hyper-conjugative interactions and electron delocalization were analyzed using NBO analysis. Intramolecular interactions were analyzed by AIM approach. The chemical reactivity descriptors were calculated to study the reactive sites within molecule.

Keywords: XRD, PED; TD-DFT; NLO; NBO

INTRODUCTION

Chalcones are open chain flavonoids, either natural or synthetic, with two aromatic rings attached by α, β-unsaturated carbonyl group [1-3]. They are synthesized by condensing aromatic ketones with aromatic aldehydes in the presence of appropriate bases through Claisen-Schmidt condensation. They acts as precursors for flavonoids in higher plants and displays wide variety of pharmacological effects including, anti-inflammatory [4], anti-malarial [5], anti-leishmanial, anti-cancer [6], antagiogenic [7] and anti-tumor [8]. For the synthesis of five- [9], six-[10] and seven-membered [11] heterocyclic compounds chalcones are used as valuable intermediate. Also they are probable new materials for optical sensors [12], UV-absorption filters [13], ultra-fast optical non-linearities [14] and non-linear optical (NLO) response [15]. NLO materials have been an area of interest to the chemists in recent years due to their future potential applications in the fields of optoelectronic such as optical communication, optical computing, optical switching and dynamic image processing [16]. Hyperpolarizability is quite useful both in understanding the relationship between the molecular structure and non-linear optical properties, which provides a guideline to experimentalists for the design and synthesis of organic NLO materials.

In the present paper we report the synthesis, crystal structure, weaker interactions, spectroscopic analysis and chemical reactivity of the title compound using experimental and quantum chemical approaches. Quantum chemical calculations have also been performed to analyze thermodynamic parameters, first static hyperpolarizability and NBO analysis. AIM approach has extensively been applied to classify and understand hydrogen bonding interactions

and ellipticity in the synthesized molecule. Local reactivity descriptors were calculated to study the reactive site within the molecule.

EXPERIMENTAL SECTION

2.1. Material and methods

All the reagents used are of analytical grade and were used as supplied. The solvent ethanol was dried and distilled before use by following the standard procedures [17].Thin layer chromatography (TLC) was performed on Silica Gel 'G' (Merck, India) coated plates for monitoring the progress of reaction. Melting point (^oC) was determined in electro- thermal melting point apparatus and was uncorrected. Elemental analysis (C, H and N) was performed on Varian Elementar –III CHN analyzer. Infrared spectrum was recorded in KBr pellets on Perkin Elmer RX-1 spectrometer from 4000 to 400 cm^{-1}. ^1H NMR spectrum of synthesized compound was recorded in $CDCl_3$ on Bruker DRX-300 MHz spectrophotometer. Chemicals shifts are given in ppm relative to (TMS) as an internal standard. UV/Visible spectra were taken on Labtronics LT-2900 spectrophotometer using quartz cell of 10 mm path length.

2.2. Synthesis of (E)-3-(4-(dimethylamino) phenyl)-1-(2-hydroxyphenyl) prop-2-en-1-one (3)

To an ice cold stirred mixture of *o*-hydroxy acetophenone (10 mmol, 1.05 mL) and *p*-dimethyl amino benzaldehyde (10 mmol, 1.49 g) in 95% ethanol (25 mL) was added 40% NaOH (15.0 mL) drop wise and reaction mixture was stirred at room temperature for about 48 h .The progress of reaction was monitored by TLC . After the completion of reaction the reaction mixture was diluted with ice cold water and neutralized with 10 % aqueous HCl and kept for overnight to obtain deep red colored precipitate. The precipitate was filtered off, washed with water-ethanol mixture and dried in air. The product was recrystallized from ethanol giving vermilion red powder, Yield: 79 %, m.p: 149-151 ºC. Anal. Calcd for $C_{17}H_{17}NO_2$ (267.32) C 76.38%, H 6.41% and N 5.24%. Found C 76.56%, H 6.63% and N 5.08%. ^1H NMR (300 MHz, $CDCl_3$) δ (ppm): 13.22 (1H, s, -OH), 7.92-7.95 (1H, d, *J* = 8.4 Hz), 7.90-7.95 (1H, d, -HC=CH-, *J* = 15.3Hz), 7.44-7.49 (1H, d, -HC=CH-, *J* = 15.3 Hz), 7.57-7.60 (2H, d, *J* = 8.9 Hz), 7.46-7.49 (1H, d, *J* = 8.4 Hz), 6.99-7.02 (1H, dd, *J* = 8.4 Hz), 6.90-6.95 (1H, dd, *J* = 8.1 Hz), 6.69-6.72 (2H, d, *J* = 8.9 Hz), 3.08 (6H,s,-$N(CH_3)_2$). IR ν_{max} (in cm^{-1}): 3071, 3022, 2998, 2912, 2865, 2848, 1618, 1531, 1487, 1433, 1376, 1312, 1280, 1203, 1155, 1030, 986, 942, 881, 812, 764, 711, 652, 510, 423.

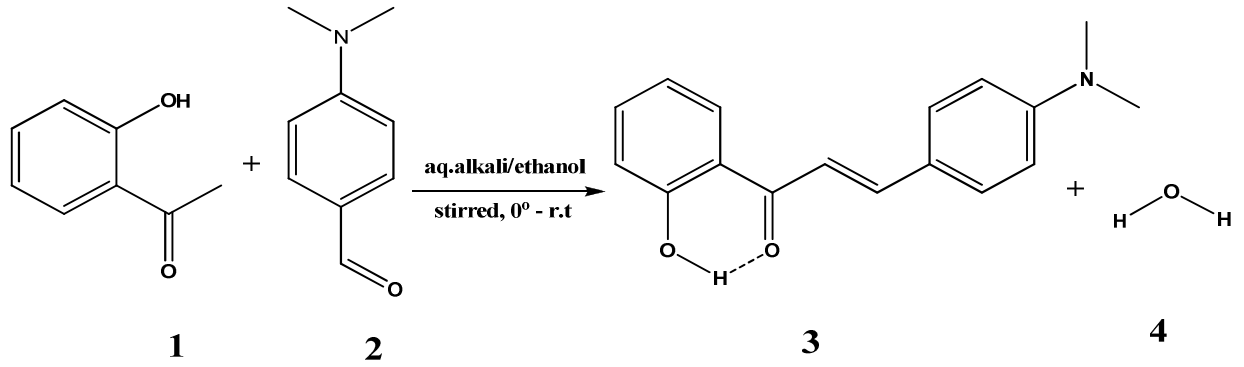

1 **2** **3** **4**

Scheme-1

2.3. X-ray crystallography

The crystal of X-ray quality for the compound was obtained by slow evaporation of ethanol/diethyl ether solvent mixture at room temperature. X-ray crystallographic data was recorded by mounting single reddish colored crystal of compound of size 0.15 x 0.20 x 0.25 mm^3 on glass fibers. Cell determination and intensity data were collected at 298(2) K on a Oxford diffraction XCALIBUR-S CCD area detector diffractometer system equipped with graphite monochromated Mo Kα radiation λ = 0.71073 Å. The final unit cell determination, scaling of data and correction for Lorentz and polarization effects were performed. Symmetry related (multi-scan) absorption correction has been applied. Structure solution by direct methods, followed by full matrix least square refinement technique on F^2 using anisotropic displacement parameters, was performed using the WINGX v 2013.3 suite [18] and SHELX-97 programs [19]. All non-hydrogen atoms were refined ansiotropically; hydrogen atoms were located at calculated positions and refined using riding model. Figures were prepared using ORTEP-3 [20]. Hydrogen bonding interactions were analyzed using PLATON [21]. Summary of crystallographic data is presented in Table 1.

Table-1: Crystal data and structure refinement

CCDC deposition number	**1041546**
Empirical formula	$C_{11.3}H_{11.3}N_{0.7}O_{1.3}$
Formula weight	178.21
Color and habit	Reddish, needle
Crystal size (mm)	0.15 x 0.20 x 0.25
Crystal system	Monoclinic,
Space group	$P2_1/c$
Temperature (K)	298(2)
Unit cell dimensions	a (Å) = 12.1175(10), α (º) = 90.00
	b (Å) = 10.2884(7), β (º) = 115.77(10)
	c (Å) = 12.4833(11), γ (º) = 90.00
Volume (A^3)	1401.51(19)
λ(Mo Kα) (Å)	0.71073
Z	4
D_C (mg m^{-3})	1.267
μ (mm^{-1})	0.083
F(000)	568.0
No. of reflection (unique)	6422/3202
No. of refined parameter	194
Data/restraints/parameters	3202 / 0 / 194
Index ranges	$-16 \le h \le 15$, $-13 \le k \le 6$, $13 \le l \le 16$
θ Range for data collection(º)	3.28 to 29.15°.
Completeness to θ	84.9 %
Absorption correction	Semi-empirical from equivalents
Max. and min. transmission	0.9877 and 0.9796
Refinement method	Full-matrix least-squares on F^2
R factor [I > 2σ (I)]	0.0474
wR2 [I > 2σ (I)]	0.1088
R factor (all data)	0.0746,
wR2(all data)	0.1255
Goodness of fit (GoF)	1.031

2.4. Computational details

All quantum-chemical calculations were carried out with Gaussian 09 program package [22] using DFT- B3LYP functional with standard 6-311G (d, p) basis set. Molecular geometry was fully optimized by Berny's optimization algorithm using redundant internal coordinates. The ^{1}H NMR chemical shifts were calculated by employing Gauge Induced atomic orbital (GIAO) method [23]. Internal coordinate system recommended by Pulay et al. was used for the assignment of vibrational modes [24]. Harmonic vibrational wave numbers were calculated using the analytic second derivatives to confirm the convergence to the minima of the potential surface. The absence of imaginary wave numbers of the calculated vibrational spectrum confirms that the deduced structure corresponds to minimum energy. Potential energy distribution along internal coordinates is calculated with the help of Gar2ped software [25]. A newly designed functional, the long range Coulomb attenuating method (CAM-B3LYP) comprising of 81% of B88 exchange at short-range and 65% of HF plus 35% of B88 at long-range [26], has been applied and was reasonably capable of predicting the excitation energies and absorption spectra of the D-π-A molecules having charge-transfer excitations [27-28]. The energies and intensities of the 30 lowest energy spin allowed electronic excitations were computed with the help of TD-DFT using CAM-B3LYP method in vacuum and also in solvents using polarized continuum model (PCM) [29]. The solvents parameters used were of dichloromethane and ethanol. Using the optimized coordinates of the compound, the first static hyperpolarizability (β_0) was calculated employing the finite field perturbation method in vacuum as well as in the solvents having different polarity using PCM model [29]. Stability of molecules as a result of hyper-conjugative interactions and electron delocalization were analyzed using natural bond orbital (NBO) analysis [30]. Presentation graphics including molecular geometries visualizations were done using Gauss view 05 [31] program. The statistical thermodynamic functions are calculated at same level of theory and basis set. The wave function obtained from the optimization was used to calculate the topological parameters at the BCPs using the Bader's theory of 'Atoms in Molecules", implemented in AIM 2000 software [32].

RESULTS AND DISCUSSION

3.1. Crystal structure

The ORTEP view of the title compound is shown in Fig.1.The crystal structure of compound shows that the molecule crystallises in monoclinic system having space group $P2_1/c$. The unit cell packing contains four molecule. The molecule is almost planar and is in *E*-configuration with respect to C=C double bond having bond length of 1.34 Å. The dihederal angle between the two aromatic rings is 10.34º. The torsion angle O1-C17-C12-C11 is -1.75º

while the torsion angles O2-C11-C12-C17 and O2-C11-C10-C9 have magnitudes -1.29º and -3.79º respectively.The unit cell packing of title compound is shown as Fig.2.

The analyses of X-ray crystal structure reveals presence of two intramolecular interactions. The hydrogen bond geometry is given in Table 2.

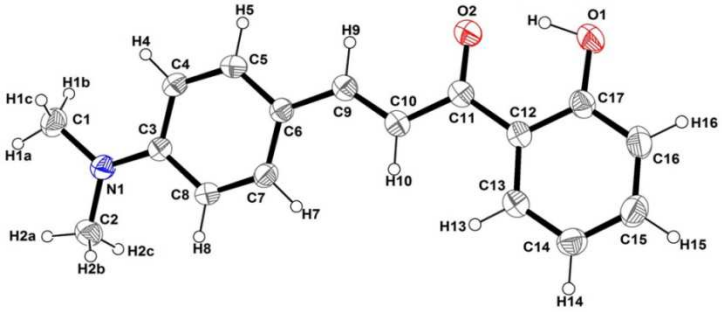

Figure-1: ORTEP view of molecule at 30% probability with atom numbering scheme

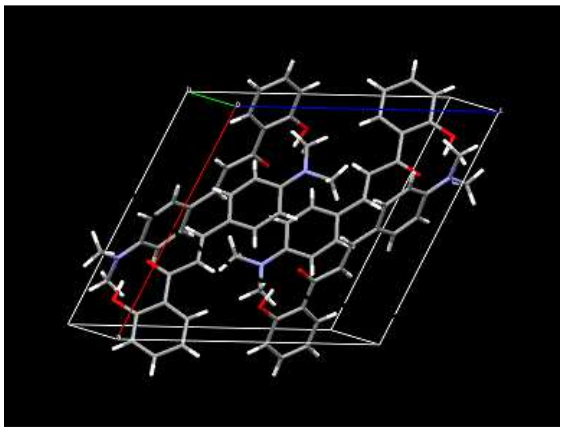

Figure-2: Unit cell packing of title compound

Table-2: Hydrogen-bond geometry for crystal structure

D-H…A	D-H(Å)	H…A(Å)	D…A(Å)	D-H…A(º)
O1-H…O2	0.99(2)	1.58(2)	2.51(2)	153.2(19)
C9-H9…O2	0.94(15)	2.46(17)	2.79(2)	100.1(12)

3.2. Reaction thermodynamics

Thermodynamic quantities were calculated using vibrational frequencies calculations for all reactants and products at room temperature (298.15 K). For simplicity reactants 1-(2-hydroxyphenyl) ethanone and 4-(dimethyl amino) benzaldehyde are abbreviated as **(1)**, **(2)** and product (*E*)-3-(4-(dimethylamino) phenyl)-1-(2-hydroxyphenyl) prop-2-en-1-one, by product water as **(3)**, **(4)** respectively. The enthalpy ($\Delta H_{Reaction}$) in Kcal/mole, Gibbs free energy ($\Delta G_{Reaction}$) in Kcal/mole and entropy change of the reaction ($\Delta S_{Reaction}$) in Cal/mole-K were calculated and arranged in Table 3. At 25 $^{\circ}$C, for non – catalyzed reaction the calculated positive values of ΔH, ΔG indicates that the reaction is endothermic and non-spontaneous at room temperature. Thermodynamic relation between equilibrium constant (K_{eq}) and Gibbs free energy change of reaction (ΔG) at temperature (T) is given as $K_{eq} = e^{-\Delta G/RT}$. Using above equation, equilibrium constant (K_{eq}) for title reaction is calculated as 2.99 x10^{-6} i.e. $K_{eq} << 1$ at room temperature. This indicates that the reaction is favored in backward direction and does not favor the forward reaction at room temperature. The reaction becomes spontaneous at elevated temperature and the temperature gap will reduce in the presence of catalyst (aq. alkali) or reflux conditions.

Table- 3: Calculated Enthalpy (H), Gibbs free energy (G) and Entropy (S) of reactants (1, 2) and products (3, 4) and for reaction, using B3LYP/6-311G (d, p) at (25 $^{\circ}$C)

Thermodynamic properties	1	2	3	4	Reaction[a]
H (Kcal/mole)	-288717.35	-300875.36	-541630.24	- 47955.57	6.90
G (Kcal/mole)	-288744.33	-300906.11	-541673.53	-47969.37	7.53
S(Cal/mole-K)	89.944	103.448	144.938	45.096	-2.52

[a] *Reaction: 1+2 (reactants) → 3+4 (products)*

3.3. Optimized geometry

The quantum chemical calculation about geometry optimization was performed by DFT –B3LYP methods at 6-311G level of basis set using Gaussian 09 program. The geometrical parameters of crystal structure of synthesized compound are taken for optimization of structure. The calculation obtained predicts an optimized geometry of the compound to the minimum potential energy hyper-surface parameter of molecular structure having no imaginary frequencies. The optimization by this method yields stable form of the title compound with C1 symmetry having energy of -863.462681 au. Optimized geometrical structure of reactants and products involved in chemical reaction is shown in Fig.3.

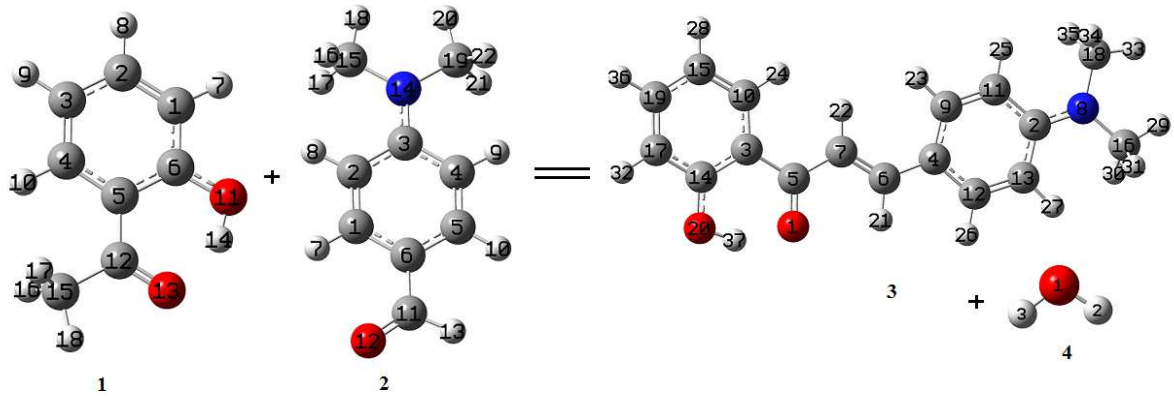

Figure-3: Optimized geometries of the reactants and products involved in chemical reaction, using B3LYP/6-311G (d, p) level of theory

Selected optimized geometrical parameters along with experimental X-ray parameters are given in Table 4. The table shows a comparison between experimental (X-ray) and calculated geometric parameters. The calculated C2–N8 bond distance of 1.37 Å and indicates that C–N bond shows partial double bond character in this fragment. Also C–N bond length are found to be much shorter than the average value for a single C–N bond (1.47Å), but significant longer than a C=N double bond (1.22Å) [33], suggesting the presence of partial double bond character. The shortening of C14-O20 bond length to 1.34 Å, also suggests the presence partial double bond character in C-O bond. The molecule is in *E*-configuration with respect to C=C bond having bond length of 1.34Å, which is in agreement with observed bond length at 1.35(2) Å. Theoretical bond lengths and bond angles are in good agreement with the experimental XRD data. When the X-ray structure of the title compound is compared with its optimized counterpart some discrepancies are observed in certain torsional angles. When the geometry of hydrogen bond in the optimized structure is examined, the proton donor group O20-H37 forms intramolecular interaction with O2 atom of carbonyl group, with bond length of 1.62Å and bond angle of 149.3º.

The discrepancies between the XRD results and the calculated geometrical parameters are due to fact that the comparison made between experimental data, obtained from solid state single crystal and calculated results are for isolated molecule in gaseous state. In spite of the differences, the calculated geometric parameters represent a good approximation and they are the basis for calculating other parameters, such as vibrational frequencies, electronic absorption spectra, molecular electrostatic parameters and other optical and spectroscopic properties.

3.4. Vibrational assignments

The observed and calculated (scaled) vibrational wave numbers at B3LYP/6-311G (d, p) level and their assignments using PED are given in Table 5. The calculated IR spectrum in the region 4000–400 cm^{-1} is shown graphically in Fig. 4. The total number of atoms in compound is 37, which give 105 (3n-6) vibrational modes. The calculated vibrational wave numbers are higher than experimental values for the majority of the normal modes. The calculated wave numbers are scaled down using single scaling factor 0.9608 to discard of any harmonicity present in real system [34]. The correlation graph is shown in Fig. 5. The value of correlation coefficient found to be r = 0.999, showing good agreement with the calculated wave numbers with experimental. Most of modes are not pure but contains significant contributions from other modes also. The potential energy distribution (PED) and modes obtained from Gauss-View program help in the assignment of the calculated harmonic vibrational wave numbers and peaks of experimental FT-IR spectrum.

Table-4: Comparison between selected optimized geometrical parameters for 3 calculated at B3LYP/6-311G (d,p) with experimental X-ray crystallographic parameters

Bond length(Å)	Calc.	Exp.	Bond angle (º)	Calc.	Exp.	Dihedral angle (º)	Calc.	Exp.
O1-C5	1.25	1.25(2)	N8-C2-C11	121.3	121.4(1)	C11-C2-N8-N16	176.7	175.2(1)
C2-N8	1.37	1.36(2)	N8-C2-C13	121.6	121.7(1)	C11-C2-N8-N18	3.6	-0.6(2)
C2-C11	1.42	1.41(2)	C11-C2-C13	117.1	116.9(1)	C13-C2-N8-C16	-3.4	-4.8(2)
C2-C13	1.41	1.40(2)	C5-C3-C10	123.3	123.1(1)	C13-C2-N8-C18	176.5	179.4(2)
C3-C5	1.48	1.48(2)	C5-C3-C14	118.8	119.3(1)	N8-C2-C11-C9	179.4	-178.6(1)
C3-C10	1.41	1.40(2)	C10-C3-C14	117.9	117.6(1)	N8-C2-C13-C12	179.4	179.0(2)
C3-C14	1.43	1.41(3)	C6-C4-C9	124.0	123.7(1)	C10-C3-C5-O1	179.8	178.6(2)
C4-C6	1.45	1.44(3)	C6-C4-C12	119.4	120.0(1)	C10-C3-C5-C7	-0.20	-2.1(2)
C4-C9	1.41	1.40(2)	C9-C4-C12	116.6	116.2(1)	C14-C3-C5-O1	-0.17	-1.3(2)
C4-C12	1.41	1.40(2)	O1-C5-C3	119.6	119.3(1)	C14-C3-C5-C7	179.8	178.0(2)
C5-C7	1.47	1.45(3)	O1-C5-C7	119.9	120.0(1)	C5-C3-C10-C15	-180.0	-179.4(2)
C6-C7	1.35	1.34(2)	C3-C5-C7	120.5	120.7(1)	C5-C3-C14-C17	-180.0	178.1(2)
N8-C16	1.45	1.45(2)	C4-C6-C7	128.4	127.9(2)	C5-C3-C14-O20	0.02	-1.8(2)
N8-C18	1.45	1.45(2)	C4-C6-C21	115.9	115.0(1)	C10-C3-C14-O20	179.6	178.4(2)
C9-C11	1.38	1.37(3)	C5-C7-C6	120.3	121.8(2)	C9-C4-C6-C7	-0.04	-3.2(3)
C10-C15	1.38	1.37(3)	C6-C7-H22	120.7	120.0(1)	C12-C4-C6-C7	179.8	179.4(2)
C12-C13	1.38	1.37(3)	C2-N8-C16	120.2	121.2(1)	C6-C4-C9-C11	180.0	-177.6(2)
C14-C17	1.40	1.39(3)	C2-N8-C18	120.3	120.9(1)	C6-C4-C12-C13	-179.9	178.1(2)
C14-O20	1.34	1.35(2)	C16-N8-C18	119.2	117.8(1)	O1-C5-C7-C6	-0.26	-3.8(3)
C15-C19	1.40	1.38(3)	C4-C9-C11	121.9	122.2(1)	O1-C5-C7-H22	179.7	175.0(1)
C17-C19	1.38	1.37(3)	C3-C10-C15	121.9	122.0(2)	C3-C5-C7-C6	179.7	176.9(2)
O20-H37	0.99	0.99(2)	C2-C11-C9	121.2	121.2(1)	C3-C5-C7-H22	-0.26	-4.0(1)
			C4-C12-C13	122.4	122.8(2)	C4-C6-C7-C5	180.0	176.4(2)
			C2-C13-C12	120.8	120.8(2)	H21-C6-C7-H22	180.0	179.0(2)
			C3-C14-C17	119.8	119.7(2)	C2-N8-C16-H29	178.3	-179.8(1)
			C3-C14-O20	122.5	122.0(2)	C2-N8-C16-H30	59.4	60.2(2)
			C17-C14-C20	117.7	118.3(2)	C2-N8-C16-H31	-61.9	-59.8(2)
			C10-C15-C19	119.3	119.4(2)	C18-N8-C16-H29	-8.5	-3.9(2)
			C14-C17-C19	120.5	120.9(2)	C18-N8-C16-H30	-127.4	-123.9(2)
			C15-C19-C17	120.6	120.4(2)	C18-N8-C16-H31	111.3	116.1(2)
			C14-O20-H37	105.9	103.0(1)	C2-N8-C18-H33	178.8	179.8(1)
						C2-N8-C18-H34	61.5	59.8(2)
						C2-N8-C18-H35	-59.9	-60.2(2)
						C16-N8-C18-H33	8.0	3.9(2)
						C16-N8-C18-H34	-111.7	-116.1(2)
						C16-N8-C18-H35	126.9	123.8(2)
						O20-C14-C17-C19	180.0	-178.3(2)
						C3-C14-O20-H37	0.08	4.0(1)
						C17-C14-O20-H37	-179.9	-176.0(1)

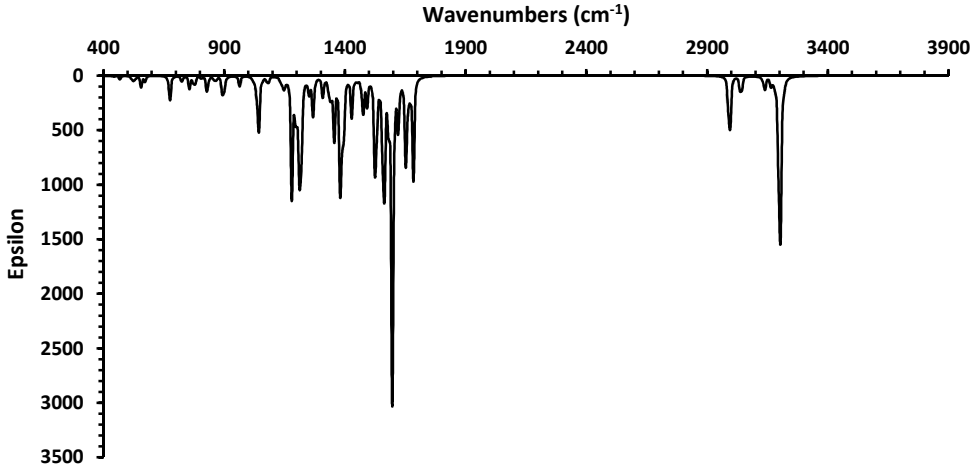

Figure-4: Calculated IR spectrum of compound 3 at B3LYP/6-311G (d, p) level

Phenolic (-OH) vibrations

The stretching vibration for phenolic (O20—H37) was observed at 3071 cm^{-1}, shows good agreement with the calculated wave number at 3076 cm^{-1}. This value is in agreement with reported value for similar compound at 3055 cm^{-1} [35]. The stretching vibration for C14—O20 was observed at 1281 cm^{-1} where as it was calculated at 1295 cm^{-}

[1]. The O-H in-plane bending vibration C14-H37-O20 was observed at 1376 cm^{-1} whereas it was found to be in good agreement with calculated wavenumber at 1372 cm^{-1}.

C—N vibrations

The observed band for C2=N8 stretching at 1487 cm^{-1} is in good agreement with the calculated value at 1499 cm^{-1} with 18% of PED. This band was also calculated at 1340 $cm^{-1}$with 28% of PED, which is not observed in experimental spectrum. Asymmetric stretching vibrations for C16-N8 and C18-N8 were calculated at 1220 cm^{-1}.This stretching vibration was not observed in experimental spectrum of title compound

C=C and C=O vibration

The C=C and C=O stretching vibrations are found to be present together. The band found at 1617 cm^{-1} is assigned to asymmetric stretching of C=C (22 % PED) and C=O (16 % PED).This mode was observed at 1618 cm^{-1} in the experimental IR spectrum. The symmetric stretching of these two bonds was calculated to be present at 1535 cm^{-1} ,which was observed at 1531 cm^{-1} with C=C (11 % PED) and C=O (22 % PED).

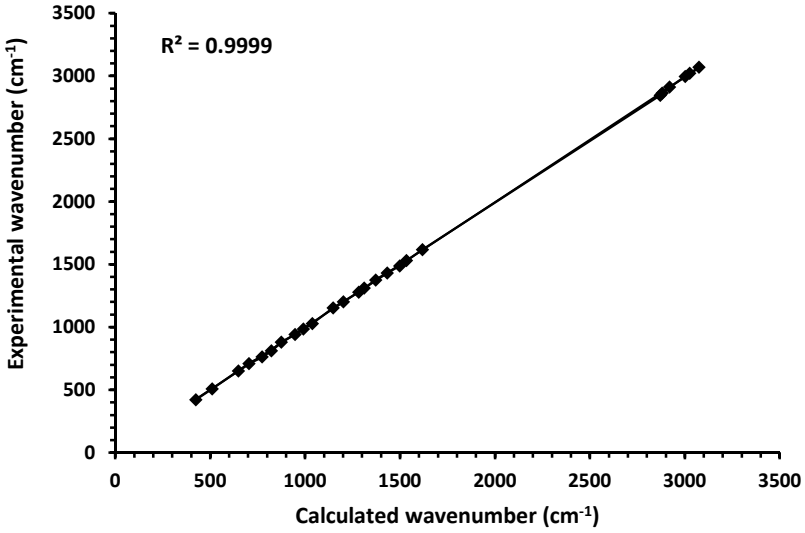

Figure-5: Correlation graph between experimental and calculated wave numbers of comp. 3

CH_3 group vibrations

According to internal coordinate system recommended by Pulay et al. [36] methyl (Me) group associate with 5 types of vibrational frequencies namely: symmetric stretch, asymmetric stretch, symmetric deformation, asymmetric deformation and rocking. The C—H stretching (symmetric and asymmetric) vibration of two CH_3 group is observed in the region 3022-2848 cm^{-1} is in agreement with the calculated wave number in region 3015- 2872 cm^{-1}. Asymmetric and symmetric deformation of Me (C16) and Me (C18) is observed at 1487 and 1433 cm^{-1} whereas the calculated value is found in region of 1474-1392 cm^{-1}. The observed methyl (C16 and C18) rocking at 1155 and 1030 cm^{-1}, agrees well with the calculated wave number at 1149 and 1039 cm^{-1}.

C—H vibrations

The aromatic C—H stretching vibrations give rise to bands in region 3100-3000 cm^{-1}. The experimental spectra show only two medium-weak band at 3071 and 3022 cm^{-1} which corresponds to C-H stretching of phenyl rings and olefinic C—H stretching [37]. These stretching bands were calculated to be found in region 3076-3015 cm^{-1}. The C—H in-plane bending vibrations are observed at 1487 and 1433 cm^{-1}, whereas it was calculated to be found in region of 1467 and 1419 cm^{-1}. Most prominent band of C—H out-of-plane bending for aromatic rings occurs in low frequency range between 942-711cm^{-1}. These values are in good agreement with calculated value in region 948-727 cm^{-1}.

Ring vibrations

The C—C stretching modes of phenyl rings are expected in the range from 1650-1200 cm^{-1}. The computed C—C stretches of phenyl rings are present at 1617, 1587, 1557, 1518, 1467, 1415 and 1258 cm^{-1}, with PED ≥ 10%. These bands are observed at 1618, 1531, 1487, 1433 and 1280 cm^{-1} in FT-IR spectrum. The series of ring deformation band (medium to weak) was observed at 986, 881, 652, 510 and 423 cm^{-1}. These deformation bands are calculated to be found at 978, 875, 649, 550 and 426 cm^{-1}.

Table -5: Experimental and calculated vibrational wave numbers (cm^{-1}) of 3 at B3LYP/6-311G (d, p) level and their assignments

modes	Calculated		Obs.	IR int.	Vibrational assignments[a] (PED ≥ 10%)
	(Unscaled)	(Scaled)			
105.	3218	3092	-	17.63	[ν(C7H22)(63)ν(C10H24)(29)]
104.	3210	3084	-	8.33	[ν(C13H27)(50)ν(C11H25)(43)]
103.	3209	3083	-	11.79	[ν(C11H25)(49)–ν(C13H27)(46)]
102.	3202	3076	3071	480.98	[ν(O20H37)(73)–ν(C10H24)(15)]
101.	3198	3073	-	165.25	[ν(C17H32)(26)–ν(C7H22)(19)ν(C15H28)(17)ν(O20H37)(15)]
100.	3194	3069	-	19.80	[ν(C17H32)(57)–ν(C10H24)(16)ν(C7H22)(10)]
99.	3183	3058	-	15.02	[ν(C15H28)(54)–ν(C10H24)(21)ν(C19H36)(12)]
98.	3175	3051	-	6.08	[ν(C9H23)(90)]
97.	3166	3042	-	14.86	[ν(C19H36)(72)–ν(C15H28)(18)]
96.	3164	3040	-	8.23	[ν(C12H26)(93)]
95.	3149	3026	3022	0.63	[ν(C6H21)(96)]
94.	3138	3015	-	45.90	[ν(C16H29)(51)ν(C18H33)(43)]
93.	3125	3003	2998	1.82	[ν(C18H33)(50)–ν(C16H29)(43)]
92.	3040	2921	2912	71.18	[ν(C18H35)(48)ν(C16H30)(27)–ν(C18H 34)(15)]
91.	3039	2920	-	6.72	[ν(C16H30)(47)–ν(C18H35)(26)–ν(C16H31)(16)]
90.	2999	2881	2865	121.04	[ν(C18H34)(39)ν(C16H31(36)ν(C18H35)(11)]
89.	2989	2872	2848	82.64	[ν(C16H31)(38)–ν(C18H34)(34)ν(C16H30)(12)–ν(C18H35)(11)]
88.	1683	1617	1618	283.12	[ν(C6C7)(22)–ν(O1C5)(16)–δ(H21C7C6)(12)]
86.	1652	1587	-	221.57	[ν(C9C11)(11)ν(C12C13)(10)]
85.	1621	1557	-	137.76	[ν(C17C19)(20)–δ(C14H 37O20)(19)–ν(C15C19)(14)–ν(C3C14)(11)]
84.	1597	1535	1531	899.44	[ν(O1C5)(22)ν(C6C7)(11)]
83.	1580	1518	-	92.63	[ν(C4C9)(19)–ν(C2C11)(15)ν(C2C13)(12)–ν(C4C12)(10)]
82.	1561	1499	1487	521.25	[ν(C2N8)(18)–δ(C4H26C12)(10)]
81.	1533	1474	-	40.14	[δ(H33H35C18)(31)δ(H29H31C16)(23)]
80.	1527	1467	-	344.97	[δ(C3H24C10)(14)–δ(C14H37O20)(14)ν(C15C19)(13)δ(C14H32C17)(12)]
79.	1519	1459	-	8.82	[δ(H29H31C16)(31)–δ(H33H35C18)(28)δ(H29H30C16)(12)]
78.	1493	1434	1433	17.01	[δ(H33H34C18)(38)–δ(H29H30C16)(27)–δ(H33H35C18)(14)]
77.	1491	1432	-	58.06	[δ(H33H34C18)(42)δ(H29H30C16)(33)]
76.	1484	1426	-	1.12	[δ(H29H30C16)(40)δ(H33H34C18)(28)-δ(H29H31C16)(13)]
75.	1477	1419	-	37.02	[δ(C15H36C19)(18)δ(C10H28C15)(16)–ν(C14O20)(12)]
74.	1473	1415	-	82.40	[ν(C12C13)(21)–ν(C9C11)(18)δ(C2H27C13)(13)–δ(H29H30C16)(11)]
73.	1449	1392	-	10.34	[δ(H29H30C16)(42)–δ(H29H30C16)(42)]
72.	1428	1372	1376	105.83	[δ(C14H37O20)(27)δ(C3H24C10)(12)]
71.	1395	1340	-	141.41	[ν(C2N8)(28)]
69.	1366	1312	1312	7.06	[δ(C16C2N8)(10)]
68.	1355	1302	-	162.33	[δ(H21C7C6)(31)δ(H21H22C6)(15)]
67.	1345	1292	-	23.81	[ν(C14O20)(23)δ(H21C7C6)(13)]
66.	1336	1284	1280	74.50	[δ(H21C7C6)(39)]
65.	1309	1258	-	54.31	[ν(C3C14)(12)ν(C14O20)(12)–ν(C3C10)(10)]
64	1270	1220	-	61.09	[ν(N8C16)(13)–ν(N8C18)(12)]
63.	1266	1216	-	61.35	[(δ-C3H24C10)(16)ν(C3C10)(10)]
62.	1251	1202	1203	43.66	[(δ-H21H22C6)(29)–(δ-C2H25C11)(11)(δ-H21C7C6)(10)]
61.	1221	1173	-	193.51	[(δ-H21H22C6)(22)–ν(C3C5)(16)ν(C14C17)(16)]
60.	1210	1163	-	322.88	[(δ-C4H26C12)(24)(δ-C4H23C9)(13)]
59.	1196	1149	1155	84.15	[(δ-H33N8C18)(25)(δ-H29N8C16)(24)]
58.	1181	1135	-	327.33	[(δ-C10H28C15)(27)–(δ-C15H36C19)(12)–(δ-C14H32C17)(11)]
57.	1155	1110	-	4.37	[(δ-C4H23C9)(12)–(δ-C2H27C13)(10)–(δ-C4H26C12)(10)]
56.	1149	1104	-	29.40	[(δ-C15H36C19)(20)ν(C10C15)(13)(δ-C14H32C17)(10)]
55.	1139	1094	-	1.19	[(δ-H34N8C18)(64)(δ-H30N8C16)(26)]
54.	1137	1092	-	24.07	[(δ-H30N8C16)(62)–(δ-H34N8C18)(28)]
53.	1081	1039	1030	27.52	[δ(H29N8C16)(31)–δ(H33N8C18)(31)ν(N8C16)(15)–ν(N 8C18)(15)]
52.	1057	1016	-	8.05	[ν(C15C19)(46)ν(C17C19)(13)–(δ-C14H32C17)(13)]
51.	1042	1001	-	197.81	[ν(C5C7)(37)(δ-$_{CC}$ PhI)(28)]
50.	1032	992	986	19.93	[(γ-C7H21H22C6)(75)]
49.	1018	978	-	8.15	[(δ-$_{CC}$ PhII)(49)]
48.	987	948	942	0.25	[(γ-H36C15C17C19)(53)(γ-H32C14C19C17)(18)–(γ-H28C10C19C15)(14)]
47.	964	926	-	26.91	[ν(N8C18)(26)ν(N8C16)(25)]
43.	911	875	881	4.05	[(δ-C6C7C5)(18)(δ-C4C6C7)(16)–(δ-$_{CC}$ PhI)(13)ν(C4C9)(10)]
42.	896	861	-	91.73	[(γ-H37O20C14C17)(84)]
41.	867	833	-	3.44	[(τ-O1C5C7H22)(26)(γ-C7H21H22C6)(25)(γ-C7O1C3C5)(17)]
40.	865	831	-	9.89	[(γ-H32C14C19C17)(35)(γ-H24C3C15C10)(16)–(τ-PhI)(13)]
39.	857	823	812	8.88	[(δ-C14C10C3)(27)ν(C14C17)(12)]
38.	830	797	-	50.84	[(γ-H27C2C12C13)(22)–(γ-H25C2C9C11)(22)(γ-N8C13C11C2)(17)]
36.	807	775	764	7.56	[(δ-C13C11C2)(14)–ν(C3C14)(12)]
35.	776	746	-	39.18	[(γ-C7O1C3C5)(20)–(τ-PhII)(12)–(τ-PhI)(12)]]
34.	757	727	-	34.50	[(γ-H28C10C19C15)(30)(γ-H24C3C15C10)(16)(γ-O20C3C17C14)(14)
33.	734	705	711	2.46	[(τ-PhII)(39)–(τ-PhI)(20)(γ-N8C13C11C2)(10)]
32.	724	696	-	13.91	[ν(C2N8)(11)–(δ-C13C11C2)(11)ν(N8C16)(10)]

31.	690	663	-	1.29	[(τ-PhI)(35)(γ-C7O1C3C5)(22)–(τ-O1C5C7H22)(11)]
30.	675	649	652	71.36	[(δ-PhI)(35)(δ-O1C3C5)(25)]
28.	572	550	-	15.07	[(δ-PhI)(49)(δ-C10C5C3)(13)]
27.	556	534	-	30.15	[(δ-C2C9C11)(21)–(δ-C16C18N8)(20)–(δ-C4C6C7)(11)]
25.	533	512	510	6.74	[(δ-O1C7C5)(15)(δ-C3O20C14)(12)[
24.	521	501	-	20.19	[(γ-N8C13C11C2)(25)(τ-PhII)(17)(γ-C6C9C12C4)(14)]
22.	468	450	-	9.63	[δ(C3O20C14)(23)δ(C16C2N8)(21)–δ(C13N8C2)(11)]
21.	443	426	423	2.28	[(δ-O1C3C5)(27)–(δ-PhI)(21)–(δ-C16C18N8)(13)ν(C3C5)(11)]
20.	437	420	-	0.36	[(τ-PhI)(42)–(τ-PhI)(18)–(γ-C5C10C14C3)(17)]
19.	432	415	-	0.20	[(τ-PhII)(76)]

[a] *abbreviations: ν - stretching; δ - in-plane deformation; γ - out-of-plane deformation; τ - torsion; as - asymmetric; s - symmetric; PhI- hydroxy substituted benzene ring; PhII - dmethylamino substituted benzene ring; % of PED is given in brackets; IR int. - IR intensity.*

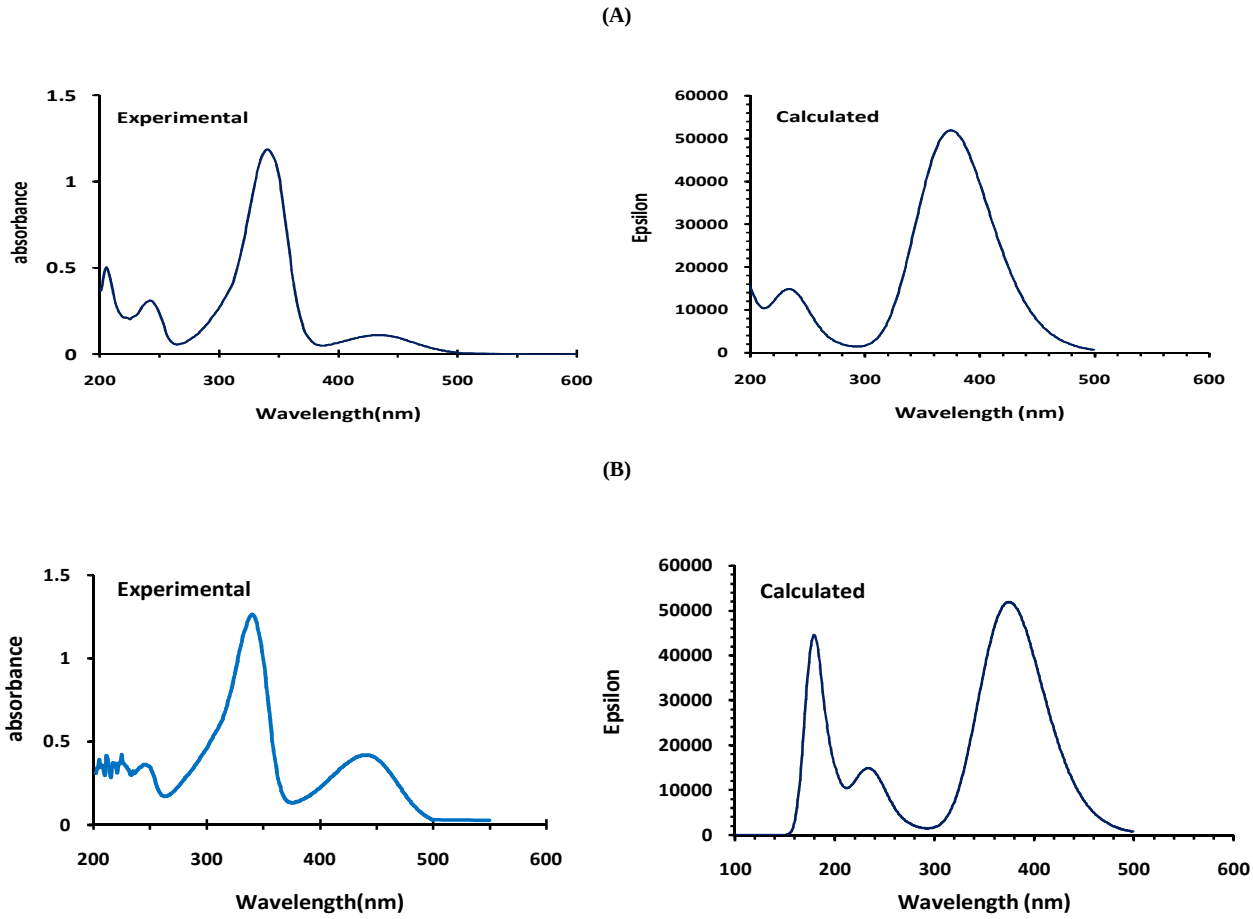

Figure-6: Experimental and calculated UV-Visible spectrum of compound 3 in solvent ethanol (A) and dichloromethane (B).

3.5. Electronic absorption spectra

To assign the nature of electronic transitions, electronic excitation energies and oscillatory strength, the UV–visible spectrum of compound has been studied by time dependent density functional theory (TD-DFT), with a hybrid exchange – correlation functional using Coulomb-attenuating method (CAM-B3LYP). The TD-DFT excitations were calculated both on gas phase and in the solvent using the IFZ-PCM model (dichloromethane and ethanol). A comparative experimental and calculated stimulated UV–Vis spectrum of compound **3** in solvent ethanol and dichloromethane is shown in Fig. 6. By comparing the calculated spectra it is evident that the calculated transitions do not exhibit significant solvatochromic effects. The observed and calculated electronic transitions of high oscillatory strength, along with experimental wavelength in ethanol and DCM are presented in Table 6. The first weak and broad experimental band of low energy near 442-436 nm was found to be absent in calculated spectrum in both the solvents. This may be due to n → π* transitions. The strong intensity band calculated near 374 nm (oscillator strength *f* = 1.28-1.30) in both the solvents is mainly due to H → L (π → π*) charge transfer transition, along charge transfer axis. This band was observed in the experimental spectrum of both solvents at 342 nm, showing significant hypsochromic shift of about 32 nm. The hypsochromic shift is occurring due to hydrogen bonding of the solvent effect [40]. The observed medium intensity band near 246-248 nm was found to be in good agreement with the calculated wavelength at 246 nm. This electronic transition is mainly due π → π* from H-3 → L

molecular orbital. The high energy transition band observed near 205-207 nm, calculated near 199-200 nm is mainly attributed to $\pi \rightarrow \pi^*$ from H-1 → L+3. The calculated electronic excitations give rise to the same pattern of bands, at energies and are in good agreements with the experimental spectrum. However, in comparison to the gas phase spectrum the band observed at 346 nm displays significant red shifting to 374 nm in dichloromethane and to 375 nm in solvent ethanol. On the basis of calculated molecular orbital coefficients analysis and molecular orbital plots for the title compound, the FMOs are mainly composed of *p*-atomic orbital's and so the nature of major electronic excitations are assigned to be $\pi \rightarrow \pi^*$ type.

Table-6: Selected TD-DFT/CAM-B3LYP excitations and their approximate assignments for compound 3

Excitation energy (eV)	Experimental λ(nm)	Calculated λ(nm)	Oscillator strength (*f*)	Major transition and expansion coefficient (CI)	Nature of transitions
In gas phase					
3.5802	-	346	1.1672	H(71) → L(72) (0.65914)	π → π*
5.6637	-	219	0.1391	H-3(68) → L(72) (0.56797)	π → π*
6.2067	-	200	0.1439	H-1(70) → L+3(73) (0.53826)	π → π*
In solvent ethanol					
3.3090	342	375	1.2820	H(71) → L(72) (0.66774)	π → π*
5.0500	246	246	0.1274	H-3(68) → L(72) (0.55226)	π → π*
5.3195	-	233	0.1048	H-2(69) → L(72) (0.56305)	π → π*
5.6795	-	218	0.1198	H-1(70) → L+1(73) (0.52794)	π → π*
6.2273	207	199	0.1796	H-1(70) → L+3(73) (0.53534)	π → π*
In solvent dichloromethane					
3.3133	342	374	1.2964	H(71) → L(72) (0.66713)	π → π*
5.0479	248	246	0.1320	H-3(68) → L(72) (0.55252)	π → π*
5.3335	-	233	0.1060	H-2(69) → L(72) (0.55512)	π → π*
5.6665	-	219	0.1271	H-1(70) → L+1(73) (0.52789)	π → π*
6.2150	205	200	0.1962	H-1(70) → L+3(73) (0.55072)	π → π*

3.6. Frontier molecular orbitals

To explain several types of reactions and for predicting the most reactive position in conjugated system, molecular orbital and their properties such as energy are used [38]. The highest occupied molecular orbital HOMO and lowest unoccupied molecular orbital (LUMO) are very popular quantum chemical parameters. The energy gap between the HOMO and LUMO is a critical parameter in determining molecular electrical transport properties because it is a measure of electron conductivity [39]. Frontier molecular orbitals (FMOs), HOMO and LUMO plots along with the other molecular orbitals plot, active in the electronic transition in solvent ethanol and their transition energy (eV) are present in Fig. 7. The energies of HOMO and LUMO are negative, which indicate the title molecule is stable [40]. The HOMO–LUMO energy gap is an important stability index. A molecule having a small frontier orbital gap is more polarizable and is generally associated with high chemical reactivity and low kinetic stability. In the title compound, HOMO is of π nature and delocalized mainly over dimethylamino substituted phenyl ring portion and olefinic double bond. By contrast LUMO is located over the hydroxy substituted phenyl rings, carbonyl group and olefinic double bond.

HOMO energy = -5.497eV
LUMO energy = -2.122eV
HOMO—LUMO energy gap = -3.375eV

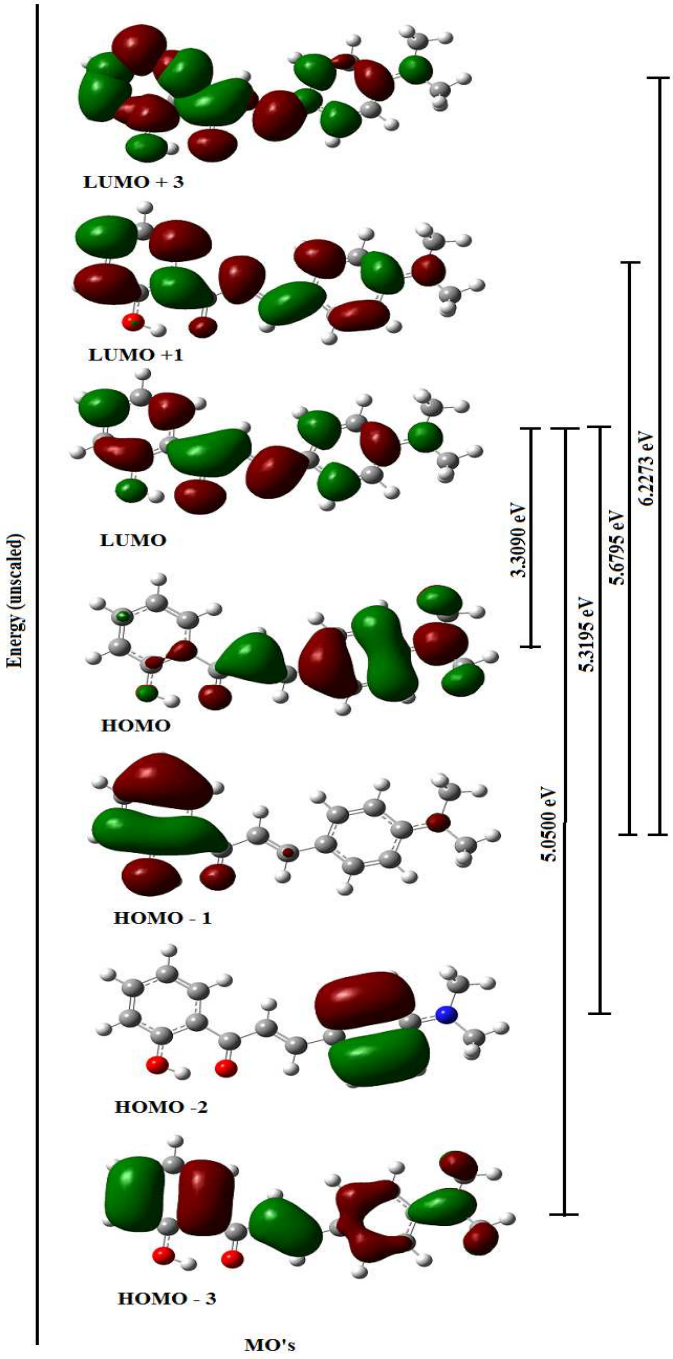

Figure-7: Selected orbital transition for 3 obtained from TD-DFT/CAM-B3LYP calculations using PCM model for ethanol

3.7. ^{1}H NMR spectroscopy

The ^{1}H NMR chemical shifts of are calculated with gauge-including atomic orbital (GIAO) approach using B3LYP method and 6-311G (d, p) basis set [41]. Chemical shift of any atom (X) is calculated as difference between isotropic magnetic shielding (IMS) of TMS and atom (X). It is defined by an equation written as: $\delta x = IMS_{TMS} - IMS_X$.

The experimental and calculated values of ^{1}H chemical shifts of the title compound are given in Table 7. The experimental ^{1}H spectrum of compound **3** shown in Fig. 8, showed one proton (H-37) singlet at δ 13.22 for phenolic –OH. Two doublet peaks observed for proton H-21 and H-22 at δ 7.90-7.95 (J = 15.3Hz) and δ 7.44-7.49 (J = 15.3Hz) respectively corresponds to olefinic (H-C=C-H) protons. The appearance of peaks at δ 7.57-7.60 (J = 8.9 Hz) and δ 6.69-6.72 (J = 8.7 Hz), corresponds to two proton doublets for H-23, 26 and H-25, 27 respectively of dimethyl amino phenyl ring. The hydroxyl phenyl ring showed two, one proton doublets for H-32 and H-24 at δ 7.46-7.49 (J = 8.4 Hz) and δ 7.92-7.95(J = 8.4 Hz).The H-36 and H-28 protons were observed as double doublets at

δ 6.99-7.02 (J = 8.4 Hz) and 6.90-6.95 (J = 8.1 Hz) respectively. Presence of 6H singlet at δ 3.08 corresponds to two methyl group protons (H-29, 30, 31, 33, 34, 34) of dimethyl amino group.

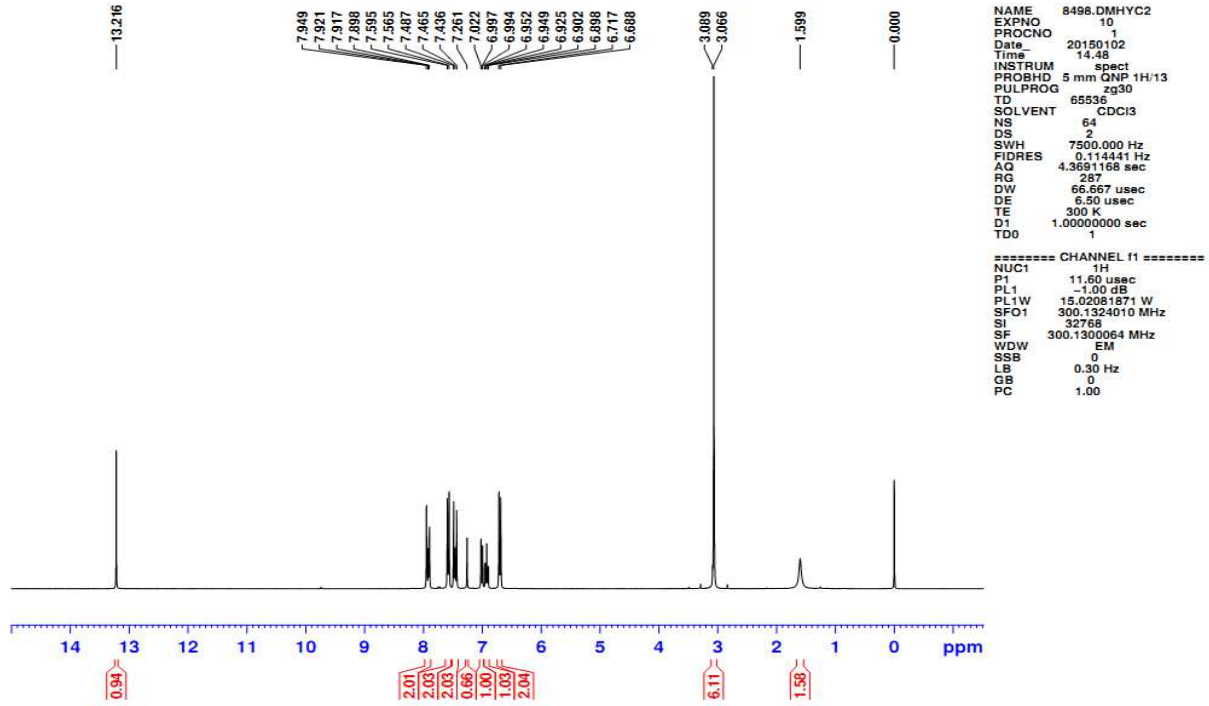

Figure-8: Experimental ^{1}H NMR spectrum of compound 3 in $CDCl_3$

Table -7: The comparison between experimental and calculated (B3LYP/6-311G/GAIO) ^{1}H NMR chemical shifts δ (ppm) from TMS and their assignments for compound 3

Atom no.	Calcd chemical shifts	Exp. chemical shifts	Assignment
37H	13.86	13.22	1H, s, phenolic (-OH)
21H	8.09	7.90-7.95	1H, d, J = 15.3Hz (-CH=CH-)
22H	7.53	7.44-7.49	1H, d, J = 15.3Hz (-CH=CH-)
23H	8.02	7.57-7.60	2H, d, J = 8.9Hz (aromatic)
26H	7.41		
25H	6.55	6.69-6.72	2H, d, J = 8.7Hz (aromatic)
27H	6.43		
32H	6.94	7.46-7.49	1H, d, J = 8.4Hz (aromatic)
36H	7.35	6.99-7.02	1H, dd, J = 8.4Hz (aromatic)
28H	6.73	6.90-6.95	1H, dd, J = 8.1Hz (aromatic)
24H	7.84	7.92-7.95	1H, d, J = 8.4Hz (aromatic)
29H, 30H, 31H	2.93	3.07	6H, s, (-N(CH_3)$_2$)
33H, 34H, 35H	2.96	3.09	

Abbreviations: s = singlet; d = doublet; dd = double doublet

In order to compare the chemical shifts correlation, graphics between the experimental and calculated ^{1}H NMR chemical shifts are shown in Fig. 9. The correlation graph follow the linear equation (y= 0.915x + 0.617); where y is the experimental ^{1}H NMR chemical shift, x is the calculated ^{1}H NMR chemical shift (in *ppm*).The value of correlation coefficient (R^2 = 0.990) shows that there is a good agreement between experimental and calculated results.

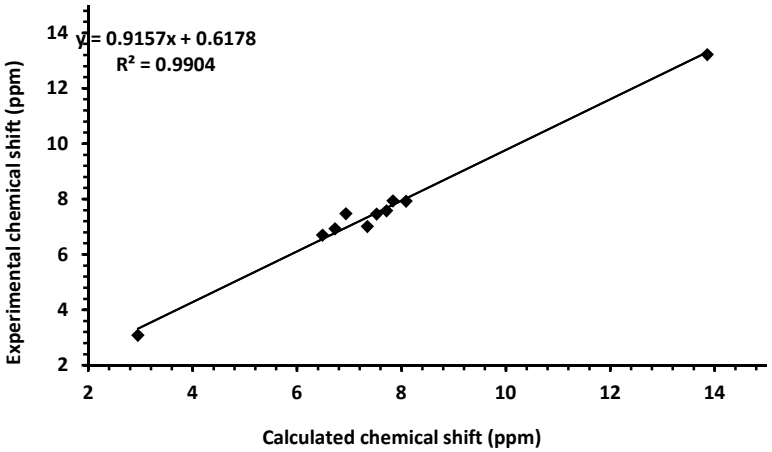

Figure-9: Correlation graphic between experimental and calculated ^{1}H NMR chemical shifts

3.8. Molecular electrostatic potential (MEP)

The MEP is related to the electron density and is very useful descriptor in determining the sites for electrophilic and nucleophilic reactions as well as hydrogen bonding interactions [42, 43]. The electrostatic potential V(r) is also is also well suited for analyzing processes based on the recognition of one molecule by another, as in drug-receptor and enzyme-substrate interactions [44]. It provides a visual method to understand the relative polarity of a molecule. The different values of electrostatic potential at the surface are represented by different colors as red represents the region of most electronegative electrostatic potential, blue represents region of most positive electrostatic potential and green represents region of zero potential. To predict reactive sites for electrophilic and nucleophilic attack for the investigated molecule, the MEP at the B3LYP/6-311G (d, p) optimized geometry was calculated. The electron density isosurface on to which the electrostatic potential surface has been mapped is shown in Fig. 10. The negative (red and yellow) regions of MEP were related to electrophilic reactivity and the positive (blue) regions to nucleophilic reactivity. From the MEP it is evident that the negative charge covers the oxygen atom of carbonyl and hydroxyl groups and some positive region is found mainly over the methyl hydrogen's. These sites give information about region where the compound can have intermolecular interactions.

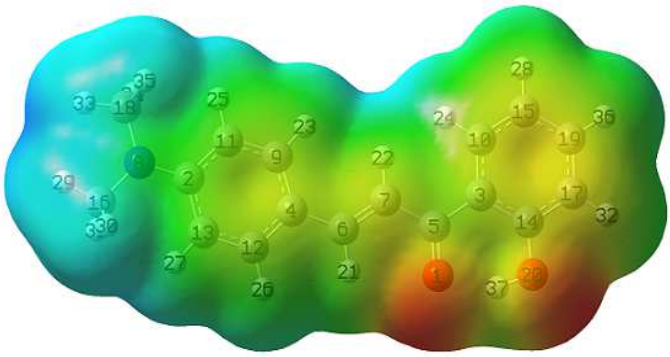

Figure-10: MEP of compound 3 showing total density mapped with ESP. (For interpretation of the references to color in this figure legend, the reader is referred to the web version)

3.9. Natural bond order analysis (NBO)

The natural bond orbital (NBO) calculations were performed using NBO 3.1 program [45] as implemented in the Gaussian 09 package at the DFT/B3LYP level in order to understand various second-order interactions between the filled orbital of one subsystem and vacant orbital of another subsystem, which is a measure of the intermolecular delocalization or hyper-conjugation. NBO analysis has an appealing aspect of highlighting the individual bonds and lone-pair energy that play a vital role in the chemical processes [46, 47]. It is an important tool for studying hybridization, covalence, hydrogen-bonding and Vander Waals interactions. In other words natural bond orbital (NBO) provides supplementary structural information. For each donor NBO (*i*) and acceptor NBO (*j*), the strength of interaction (or stabilization energy) E (2) associated with electron delocalization between donor and acceptor is estimated by the second order energy lowering as [48]

$$E^{(2)} = \Delta E_{ij} = q_i \frac{(F_{ij})^2}{(\varepsilon_j - \varepsilon_i)}$$

Where, q_i is donor orbital occupancy; ε_i, ε_j are orbital energies (diagonal elements), F_{ij} is the off-diagonal Fock or Kohn–Sham matrix element. The higher value of E (2) points toward the greater interaction between electron donors and electron acceptors (i.e. the more donating tendency from electron donors to electron acceptors and the greater the extent of conjugation in the system).

Second-order perturbation theory analysis for selected donor (Lewis) and acceptor (non-Lewis) orbitals of the Fock matrix in NBO basis is presented in Table 8. The π-conjugation/resonance due to π-electron delocalization is involved due to the π-π* interactions whereas, the primary hyper conjugative interactions due to the various types of orbital overlaps such as σ-π*, π-σ* n-σ* and secondary hyper conjugative interactions due to the orbital overlap σ-σ*. A very strong interaction have been observed between *p* type orbital containing lone pair of n_2 (O20) with the neighbour π*(C14-C17) anti-bonding orbital of hydroxy phenyl ring. This interaction is responsible for a pronounced decrease of the lone pair orbital occupancy and increases anti-bonding π*(C14-C17) ED to 0.38019e and is responsible for shortening of C14-O20 bond length to 1.34Å, leading to multiple bond character between C14-O20 bond. Such high energy interaction involving lone pair of electron, leads to stabilization of molecule up to 38.36 kcal/mol. Other important primary hyper-conjugative interactions involving lone pairs are given in table.

The intermolecular hyper-conjugative interactions are formed by the orbital overlap between π → π* bond orbital, which results intra-molecular charge transfer (ITC) causing stabilization of the system. The hyper-conjugative interactions of π (C3-C10) → π*(C15-C19)/π*(C14-C17)/ π*(C1-C5), π (C14-C17) → π*(C15-C19)/π*(C3-C10), π (C15-C19) → π*(C14-C17)/π*(C3-C10) are responsible for conjugation of respective π bonds of hydroxyl phenyl ring. The electron density (ED) at the conjugation of π bonds (1.57470-1.64571e) of hydroxyl phenyl ring and π* bonds (0.30452-0.43216e), indicates strong π delocalization within the ring and with conjugated C (5) = O (1) bond leading stabilization of molecule in range of 27.67-16.35 kcal/mol. The hyper-conjugative interactions of π (C4-C12) → π*(C9-C11)/π*(C6-C7)/ π*(C2-C13), π (C2-C13) → π*(C9-C11)/π*(C4-C12), π (C9-C11) → π*(C2-C13)/π*(C4-C12) are responsible for conjugation of respective π bonds of dimethyl amino phenyl ring. The electron density (ED) at the conjugation of π bonds (1.60186-1.74239e) of dimethyl amino phenyl ring and π* bonds (0.15093-0.43504e), indicates strong π delocalization within the ring and with conjugated C (6) = C (7) bond leading stabilization of molecule in range of 26.54-14.29 kcal/mol. The interactions π (C6-C7) → π*(C4-C12)/π*(O1-C5) are also stabilizes the molecule in the range of 24.5-11.33 kcal/mol. stabilization of the system. The movement of π-electron cloud from donor to acceptor i.e. intra-molecular charge transfer (ICT) can make the molecule more polarized and the ICT must be responsible for the NLO properties of molecule. Therefore, the titled compound may be used for non-linear optical materials application in future.As shown in table, there are number of secondary hyper-conjugative interactions (σ → σ*) which stabilizes the molecule maximum up to 5.46 kcal/mol.

3.10. Chemical reactivity

Global reactivity descriptors

For understanding various aspects of pharmacological sciences including drug design and possible eco-toxicological characteristics of the drug molecules, several new chemical reactivity descriptors have been proposed. The chemical reactivity and site selectivity of the molecular systems have been determined by the conceptual density functional theory [49].Electronegativity (χ), chemical potential (μ), global hardness (η), global softness (S) and electrophilicity index (ω) are global reactivity descriptors, highly successful in predicting global reactivity trends. On the basis of *Koopman's theorem* [50], global reactivity descriptors are calculated using the energies of frontier molecular orbital's HOMO and LUMO.

According to Parr et al., electrophilicity index (ω) [51] is a global reactivity index which measures the stabilization in energy when the system acquires an additional electronic charge (ΔN) from the environment. The direction of the charge transfer is completely determined by the electronic chemical potential of the molecule because an electrophile is a chemical species capable of accepting electrons from the environments; its energy must decrease upon accepting electronic charge. Therefore its electronic chemical potential must be negative. The energies of frontier molecular orbitals (E_{HOMO}, E_{LUMO}), energy band gap (E_{HOMO}-E_{LUMO}), electro negativity (χ), chemical potential (μ), global hardness (η), global softness (S) and global electrophilicity index (ω) for **1**, **2** and **3** are listed in Table 9.

When two molecules react, which one will act as an electrophile (nucleophile) will depend upon higher (lower) value of electrophiicity index. The high value of electrophilicity index shows that product **(3)** is stronger electrophile than reactants **1**. Electrophilic charge transfer (ECT) is defined as the difference between the ΔN max values of interacting molecules. If we consider two molecules **1** and **2** approach to each other (i) if ECT > 0, charge flows

from **2** to **1** (ii) if ECT < 0, charge flows from **1** to **2**. ECT is calculated using equation ECT = $(\Delta N\ max)_1$ - $(\Delta N\ max)_2$, where $(\Delta N\ max)_1 = -(\mu/\eta)_1$ and $(\Delta N\ max)_2 = -(\mu/\eta)_2$. ECT is calculated as 0.281 for reactant molecules **1** and **2**, which strongly indicates that charge flows from molecule **2** to **1**. Therefore, **2** act as very strong electron donor and **1** as electron acceptor. The high value of chemical potential and low value of electrophilicity index (ω = 2.752 eV) for **2** favor its strong nucleophilic behavior. In the same way, the low value of chemical potential and high value of electrophilicity index (ω=3.886 eV) for **1** favor its electrophilic behavior.

Table- 8: Second order perturbation theory analysis of Fock matrix in NBO basis of compound 3 for selected donor (Lewis) and acceptor (non-Lewis) orbitals

Donor(*I*)	Type	Occupancy	Acceptor(*J*)	Type	Occupancy	(E^2) [a](kcal/mol)	E(*j*)-E(*i*) [b](a.u)	F(*i j*) [c](a.u)
C2-C13	π	1.60186	C9-C11	π*	0.29341	14.29	0.29	0.059
	π	1.60186	C4-C12	π*	0.41594	26.54	0.29	0.078
C3-C10	π	1.64571	C15-C19	π*	0.38873	16.64	0.28	0.061
	π	1.64571	O1-C5	π*	0.30452	26.56	0.26	0.075
	π	1.64571	C14-C17	π*	0.38019	23.28	0.28	0.072
C4-C12	π	1.61089	C9-C11	π*	0.29341	22.56	0.28	0.072
	π	1.61089	C6-C7	π*	0.15093	20.45	0.29	0.073
	π	1.61089	C2-C13	π*	0.43504	17.79	0.26	0.062
C6-C7	π	1.82079	C4-C12	π*	0.41594	11.33	0.30	0.055
	π	1.82079	O1-C5	π*	0.30452	24.75	0.27	0.076
C9-C11	π	1.74239	C2-C13	π*	0.43504	20.72	0.28	0.071
	π	1.74239	C4-C12	π*	0.41594	14.40	0.29	0.060
C14-C17	π	1.57470	C15-C19	π*	0.38873	27.67	0.28	0.079
	π	1.57470	C3-C10	π*	0.43216	16.35	0.27	0.060
C15-C19	π	1.62354	C14-C17	π*	0.38019	17.23	0.27	0.061
	π	1.62354	C3-C10	π*	0.43216	26.97	0.27	0.078
O1-C5	π	1.97149	C3-C10	π*	0.43216	4.36	0.39	0.041
LP(O20)	n_2	1.80131	C14-C17	π*	0.38019	38.36	0.33	0.105
	n_1	1.97320	C3-C14	σ*	0.03783	7.79	1.09	0.083
LP(N8)	n_1	1.69895	C16-H31	σ*	0.02042	6.41	0.63	0.061
	n_1	1.69895	C18-H34	σ*	0.02036	6.38	0.63	0.061
	n_1	1.69895	C18-H35	σ*	0.01731	5.05	0.63	0.054
	n_1	1.69895	C16-H30	σ*	0.01720	4.99	0.63	0.054
LP(O1)	n_1	1.96738	C3-C5	σ*	0.05270	4.97	1.11	0.067
C2-C11	σ	1.97013	C2-C13	σ*	0.02456	4.03	1.23	0.063
	σ	1.97013	N8-C16	σ*	0.01584	4.16	1.03	0.059
C2-C13	σ	1.97011	C2-C11	σ*	0.02486	4.01	1.23	0.063
	σ	1.97011	N8-C18	σ*	0.01587	4.16	1.03	0.059
C5-C7	σ	1.97688	C4-C6	σ*	0.02425	4.07	1.18	0.062
C6-H21	σ	1.97372	C4-C9	σ*	0.02851	5.14	1.06	0.066
	σ	1.97372	C7-H22	σ*	0.01804	5.46	0.95	0.064
C7-H22	σ	1.97905	C6-H21	σ*	0.01886	4.03	0.97	0.056
C9-H23	σ	1.97803	C2-C11	σ*	0.02486	4.79	1.05	0.063
	σ	1.97803	C4-C12	σ*	0.02400	4.12	1.08	0.060
C10-H24	σ	1.97772	C3-C14	σ*	0.03783	4.45	1.05	0.061
C11-H25	σ	1.97664	C4-C9	σ*	0.02851	4.45	1.08	0.062
C12-H26	σ	1.97827	C2-C13	σ*	0.02456	4.69	1.05	0.063
	σ	1.97827	C4-C9	σ*	0.02851	4.30	1.07	0.061
C13-H27	σ	1.97639	C2-C11	σ*	0.02486	4.05	1.05	0.058
	σ	1.97639	C4-C12	σ*	0.02400	4.35	1.08	0.061
C17-H32	σ	1.97666	C3-C14	σ*	0.03783	4.48	1.03	0.061
C18-H33	σ	1.99033	C2-N8	σ*	0.03363	4.38	1.01	0.060
C19-H36	σ	1.97925	C14-C17	σ*	0.02548	4.20	1.07	0.060

[a] *Energy of hyper conjugative interactions(stabilization energy)*
[b] *Energy difference between donor i and acceptor j NBO orbitals.*
[c] *Fock matrix element between (i) and (j)NBO orbitals.*

Table-9: Calculated E_{HOMO}, E_{LUMO}, band gap ($E_H - E_L$), chemical potential (μ), electronegativity (χ), global hardness (η), global softness (S) and global electrophilicity index (ω) (in eV) for reactants 1, 2, product 3 at B3LYP/6-311G (d, p) level

	E_{HOMO}	E_{LUMO}	$E_H - E_L$	χ	μ	η	S	ω
Reactant **(1)**	-6.422	-1.932	-4.490	4.177	-4.177	2.245	0.223	3.886
Reactant **(2)**	- 5.687	- 1.279	-4.408	3.483	-3.483	2.204	0.227	2.752
Product **(3)**	-5.497	-2.122	-3.375	3.809	-3.809	1.688	0.296	4.299

Local reactivity descriptors

Fukui function is one of the widely used local density functional descriptors to model chemical reactivity and selectivity. Local reactivity descriptors such as local softness (S_k), Fukui function (f_k) and local electrophilicity

index (ω_k) [52] have been used in DFT theory for defining the reactive site within a particular molecule. Fukui function f(r)is considered as one of the most fundamental indicator for defining the site selectivity in a given molecular species and soft-soft type of interactions, the preferred reactive site in a molecule is the one with maximum values of (f_k, S_k, ω_k) [53]. Using Hirshfeld atomic charges of neutral, cation and anion state of product **(3)** Fukui functions (f_k^+, f_k^-, f_k^0), local softnesses (s_k^+, s_k^-, s_k^0) and local electrophilicity indices ($\omega_k^+, \omega_k^-, \omega_k^0$) were calculated. Fukui functions, local softnesses and local electrophilicity indices for selected atomic sites in product **(3)** using Hirshfeld atomic charges have been listed in Table 10.

The maximum value of local nucleophilic reactivity descriptors (f_k^- , s_k^-, ω_k^-) in order O1 > O20 > N8, indicates that these sites are prone to electrophilic attack.The maximum values of local electrophilic reactivity descriptors (f_k^+ , s_k^+, ω_k^+) at carbon C-5, C-16, C-18 for **(3)** indicate that this site is more prone to nucleophilic attack. The calculated relative local electrophilic reactivity descriptors at C-5 for synthesized molecule favor the formation of new heterocyclic compounds such as pyrazoline and oxazoline.

Table-10: Selected electrophilic reactivity descriptors (f_k^+, s_k^+, ω_k^+) and nucleophilic reactivity descriptors (f_k^-, s_k^-, ω_k^-) of product 3 using Hirshfeld atomic charge at B3LYP/6-311G (d, p) level

Atom no.	f_k^+	f_k^-	s_k^+	s_k^-	ω_k^+	ω_k^-
O1	-0.22495	-0.316077	-0.06658	-0.09356	-0.96705	-1.35882
C5	0.14855	0.06239	0.04397	0.01847	0.63862	0.26821
C6	0.06800	-0.06208	0.02013	-0.01838	0.29235	-0.26688
C7	0.04742	-0.08975	0.01403	-0.02657	0.20388	-0.38584
N8	-0.00599	-0.13597	-0.00177	-0.04025	-0.02574	-0.58454
C16	0.19854	0.03253	0.05877	0.00963	0.85351	0.13986
C18	0.19718	0.03649	0.05837	0.01080	0.84769	0.15686
O20	-0.01186	-0.15278	-0.00351	-0.04522	-0.05099	-0.65682

3.11. Dipole moment (μ_0), mean polarizability ($|\alpha_0|$), anisotropy of polarizability ($\Delta\ \alpha$) and first static hyperpolarizability (β_0)

Nonlinear optics deals with the interaction of applied electromagnetic fields in various materials to generate new electromagnetic fields, altered in wave number, phase, or other physical properties [54]. Organic molecules able to manipulate photonic signals efficiently are of importance in technologies such as optical communication, optical computing, and dynamic image processing [55]. DFT has been extensively used as an effective method to investigate NLO properties of organic materials. In order to gain insight into NLO property of title compound, the first static hyperpolarizability (β) were calculated by the finite field perturbation method in vacuum as well as incorporating the solvent factors with increasing polarity. First hyperpolarizability is a third rank tensor that can be described by a 3 × 3 × 3 matrix. The 27 components of the 3D-matrix can be reduced to 10 components due to the Kleinman symmetry [56]. The components of β are defined as the coefficients in the Taylor series expansion of the energy in the external electric field. When the external electric field is weak and homogeneous this expansion becomes:

$$E = E^0 - \mu_i F_i - 1/2\alpha_{ij} F_i F_j - 1/6\beta_{ijk} F_i F_j F_k + 1/24\gamma_{ijkl}$$

Where E^0 is the energy of the unperturbed molecules, F_i the field at the origin and μ_i, α_{ij} and β_{ijk} are the components of dipole moment, polarizability, and the first hyperpolarizability respectively. Using the x, y and z components of β obtained from Gaussian 09 output, the magnitude of the mean first hyperpolarizability tensor can be calculated. The total static dipole moment (μ_0), the mean polarizability ($|\alpha_0|$), the anisotropy of the polarizability ($\Delta\ \alpha$) and the total static first hyperpolarizability (β_0) using x, y, z components are defined as using equations below:

$$\mu_0 = \left(\mu_x^2 + \mu_y^2 + \mu_z^2\right)^{1/2}$$
$$|\alpha_0| = 1/3\left(\alpha_{xx} + \alpha_{yy} + \alpha_{zz}\right)$$

$$\Delta\ \alpha = 2^{-1/2}\left[(\alpha_{xx} - \alpha_{yy})^2 + (\alpha_{yy} - \alpha_{zz})^2 + (\alpha_{zz} - \alpha_{xx})^2\right]^{1/2}$$
$$\beta_0 = (\beta_x^2 + \beta_y^2 + \beta_z^2)^{1/2}$$

Where

$$\beta_x = \beta_{xxx} + \beta_{xyy} + \beta_{xzz}$$
$$\beta_y = \beta_{yyy} + \beta_{yxx} + \beta_{yzz}$$
$$\beta_z = \beta_{zzz} + \beta_{zxx} + \beta_{zyy}$$

Since the x, y, z components of $|\alpha_0|$, Δ α, and β_0 of Gaussian 09 output are reported in a atomic mass unit (au), the calculated values have been converted into electrostatic unit (esu) using (for α_0:1 au = 0.1482 x 10^{-24} esu; for β_0: 1 au

= 0.0086393 x 10^{-30} esu). The dipole moment (μ_0), polarizability ($|\alpha_0|$), anisotropy of polarizability ($\Delta\alpha$) and first static hyperpolarizability (β_0) are calculated at B3LYP/6-311G (d, p) level and presented in Table 11. The calculated first hyperpolarizability (β_0) of the title compound in vaccum is 2.63 x10^{-30} esu, which is comparable with the reported values of related compounds [57].The β_0 value is about 3.2 times more than the β_0 magnitude of standard p-nitro aniline ($\beta_0 = 0.83 \times 10^{-30}$ esu) and 20.2 times than that of standard NLO material urea(0.13×10^{-30} esu). The β_0 value was found to increase monotonically with increase in polarity of solvent. As evident from the UV-Vis spectrum and the TD-DFT results the electronic transitions are mainly of $\pi \rightarrow \pi^*$type operating through the charge transfer axis. This charge transfer transitions are responsible for good first order NLO response in the title compound. We conclude that the title compound is an attractive object for future studies of nonlinear optical properties.

Table-11: Dielectric constant (ε) for solvents, dipole moment (μ_0) (Debye), polarizability (α_0) (10^{-24}esu), anisotropy of polarizability ($\Delta\alpha$) (10^{-24}esu) and calculated first static hyperpolarizability (β_0) (10^{-30} esu)

Medium	ε	μ_0	α_0	$\Delta\alpha$	β_0
Vacuum	-	8.23	-16.04	4.81	2.63
Dichloromethane	4.90	10.40	-15.57	5.89	3.20
Ethanol	24.30	10.69	-15.50	6.02	3.27
Acetonitrile	36.64	10.75	-15.49	6.04	3.32

3.12. AIM calculations

Geometrical as well as topological parameters are useful tool to characterize the strength of hydrogen bond. The geometrical criteria for the existence of hydrogen bond are frequently considered as insufficient, the existence of hydrogen bond could be supported further by *Koch and Popelier* criteria [58] based on *'Atoms in Molecules'* theory (i) The existence of bond critical point for the 'proton (H)-acceptor (A)' contact as a confirmation of the existence of hydrogen bonding interaction (ii) The value of electron density ρ (H…A) should be within the range 0.002–0.035 au. The corresponding Laplacian $\nabla^2\rho_{(BCP)}$ should be within the range 0.024–0.139 au. According to *Rozas et al.* [59] the interactions may be classified as follows: (i) Strong H-bonds are characterized by $\nabla^2\rho_{(BCP)} < 0$; $H_{(BCP)} < 0$; $E_{HB} > 24.0$ kcal/mol and their covalent character is established (ii) medium H-bonds are characterized by $\nabla^2\rho_{(BCP)} > 0$; $H_{(BCP)} < 0$; $12.0 < E_{HB} < 24.0$ kcal/mol and their partially covalent character is established (iii) weak H-bonds are characterized by $\nabla^2\rho_{(BCP)} > 0$; $H_{(BCP)} > 0$; $E_{HB} < 12.0$ kcal/mol and they are mainly electrostatic and the distance between interacting atoms is greater than the sum of Vander Waal's radii of these atoms.

Molecular graph of the compound **3**, using AIM program at B3LYP/6-311G (d, p) level is shown in Fig. 11. Geometrical as well as topological parameters for bonds of interacting atoms are given in Table 12. The various type of interactions visualized in molecular graph are classified on the basis of geometrical, topological and energetic parameters. In this article, the *Bader's theory* application is used to estimate hydrogen bond energy (E). Espinosa [60] proposed proportionality between hydrogen bond energy (E) and potential energy density (V_{BCP}) at H—O contact: $E = ½(V_{BCP})$. As seen from molecular graph, one intra-molecular H-bond was found to be present between O1… H37. According to AIM calculations, the energy of intra-molecular H-bond was calculated as -16.63 kcal/mol. The ellipticity (ε) at BCP is a sensitive index to monitor the π-character of bond. The ε is related to λ_1 and λ_2, which correspond to the eigen values of Hessian and defined by relationship: $\varepsilon = (\lambda_1/\lambda_2) - 1$. The ellipticity (ε) of bonds of two phenyl rings , C3-C5, C5-C7, C5-C1, C6-C7, C6-C4 and C2-N8 of title molecule at BCP are in range of 0.1006-0.2497.The lower values of ellipticity (ε) confirm that that there is strong delocalization of electron molecule. The intra-molecular hydrogen bond between O1… H37 provides extra stability to molecule, resulting in formation of six membered cyclic ring. The ellipticity value bonds C5-C1, C3-C5, C14-C3, C14-O20, O20-H37 and H37-O1 of this pseudo-ring were 0.0084, 0.1006, 0.1835, 0.0036, 0.0105 and 0.0039 respectively. This lower ellipticity values confirms the presence of resonance assisted intra-molecular hydrogen bond between O1… H37.

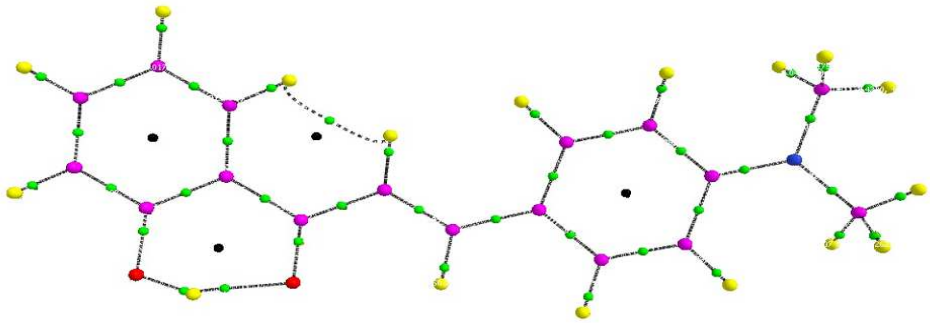

Figure-11: Molecular graph of compound 3 at B3LYP/6-311G (d, p) level using AIM program: bond critical points (small green spheres), ring critical points (small black spheres) and bond path (black lines). (For interpretation of the references to color in this figure legend, the reader is referred to the web version)

Table-12: Geometrical parameters (bond length) and topological parameters for bonds of interacting atoms: electron density $\rho_{(BCP)}$, Laplacian of electron density $\nabla^2\rho_{(BCP)}$, ellipticity(ε), electron kinetic energy density $G_{(BCP)}$, electron potential energy density $V_{(BCP)}$, total electron energy density $H_{(BCP)}$ at bond critical point (BCP) and estimated intramolecular interaction energy ($E_{int.}$) of compound 3

Interaction	Bond length	$\rho_{(BCP)}$	$\nabla^2\rho_{(BCP)}$	ε	$G_{(BCP)}$	$V_{(BCP)}$	$H_{(BCP)}$	$E_{int.}$
H22 … H24	1.958	0.011	0.045	0.705	0.009	-0.006	-0.003	–1.88
O1…H37	1.619	0.035	0.149	0.004	0.045	-0.053	0.008	–16.63

3.13. Statistical thermodynamics

On the basis of vibrational analysis and statistical thermodynamics, the standard thermodynamics functions: heat capacity $C^0_{p,m}$ entropy S^0_m and enthalpy H^0_m were obtained at B3LYP/6-311G (d, p) and are listed in Table 13. It is found that the standard heat capacities, entropies and enthalpy changes are increasing with temperatures ranging from 100 to 700 K due to the fact the molecular vibrational intensities are increasing with temperatures. The correlation equations between heat capacities, entropies, enthalpy changes and temperatures were fitted by quadratic formula. The corresponding fitting factors (R^2) for these thermodynamic properties are 0.999 (for enthalpy), 0.999 (for heat capacity) and 1.000 (for entropy) respectively. Correlation graphs of thermodynamic functions vs. temperature (T) are shown in Fig.12. The corresponding fitting equations between thermodynamic properties and temperature are as follows:

$$H^0_m = 188.4 + 0.013T + 9X10^{-5}T^2, (R^2 = 0.999)$$
$$C^0_{p,m} = 11.35 + 0.256T - 9X10^{-5}T^2 (R^2 = 0.999)$$
$$S^0_m = 66.10 + 0.282T - 6X10^{-5}T^2 (R^2 = 1.000)$$

These equations can be used to compute other thermodynamic functions and can estimate the directions of chemical reactions according to the second law of thermodynamics in thermo-chemical field [61].These equations will be helpful for the further studies of the title compound. As all thermodynamic calculations were done in gas phase and they could not be used in solution.

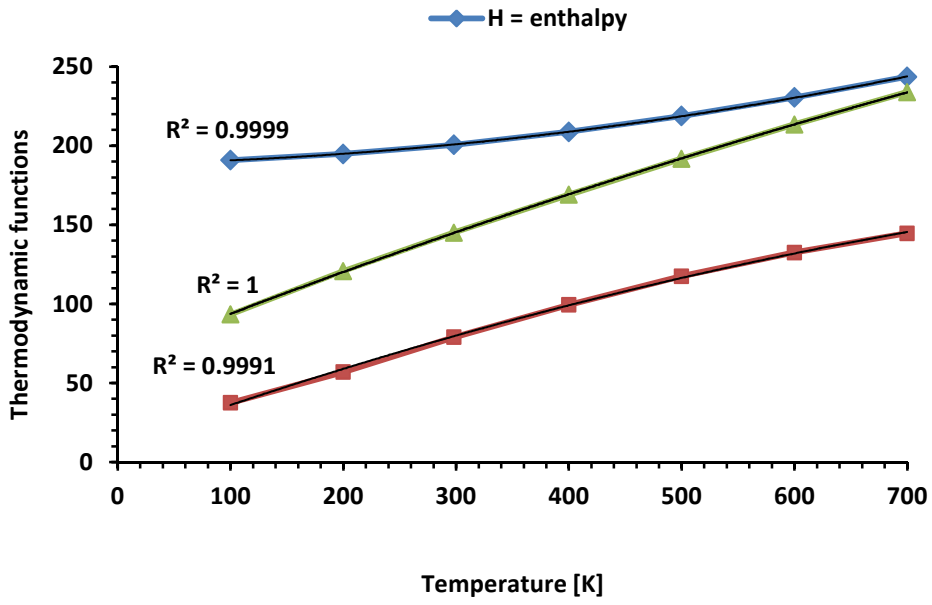

Figure-12: Correlation graphics between heat capacity, entropy and enthalpy with Temp. (K)

Table-13: Thermodynamic properties of compound 3 at different temperatures

Temperature (K)	H^0_m(kcal/mol)	$C^0_{P,m}$(cal/mol–K)	S^0_m(cal/mol –K)
100	190.939	37.502	93.368
200	194.813	56.964	120.827
298.15	200.619	79.05	145.057
400	208.823	99.425	169.073
500	218.869	117.574	191.859
600	230.566	132.495	213.487
700	243.614	144.678	233.902

CONCLUSION

The title compound was synthesized following Claisen-Schmidt condensation reaction and the structure of this compound was confirmed by IR, ^{1}H NMR, UV-Vis spectroscopy and single crystal X-ray diffraction. The structure was optimized by DFT using B3LYP/6-311G basis set and geometrical parameters are in good agreements with XRD results. The vibrational wave numbers were examined theoretically and the normal modes were assigned by potential energy distribution calculation. The UV-Vis spectrum studied by TD-DFT/CAM-B3LYP was reasonably capable of predicting the excitation energies and the absorption spectra of the molecule. The molecular orbital coefficients analyses suggest that the electronic transitions are mainly $\pi \rightarrow \pi^*$. The calculated HOMO-LUMO band gap shows the chemical reactivity of the molecule. Using NBO analysis the stability of the molecule arising from hyper-conjugative interaction and charge delocalization through π-conjugated bridge has been analyzed. A computation of the first hyperpolarizability indicates that compound may be a good candidate as a NLO material. The calculated relative value of local reactivity descriptors (f_k^+, s_k^+, ω_k^+) at **C-5** indicate that this site is more prone to nucleophilic attack. Thus, synthesized molecule **3** may be used as intermediate for the synthesis of new heterocyclic compounds such as pyrazoline and oxazoline. Intramolecular interactions and ellipticity studied by AIM approach confirms the presence of resonance assisted intramolecular hydrogen bond of medium strength between O1… H37.

Acknowledgements
The authors thankfully acknowledge the UGC New Delhi (major research project F.No.39-701/2010-SR) for financial support. We are grateful to SAIF division of the Central Drug Research Institute, Lucknow for providing spectral measurements facilities. We are also thankful to our department for providing center facility for computational research.

REFERENCES

[1] HP Avila; EFA Smania; FD Monache; A Smania*; Bioorg. Med. Chem*., **2008**, 16, 9790.
[2] M Cabrera; M Simoens; G Falchi; M L Lavaggi; OE Piro; EE Castellano; A Vidal; A Azqueta; A Monge; A L de Cerain; G Sagrera; G Seoane; H Cerecetto; M Gonzalez; *Bioorg. Med. Chem*., **2007, 15**, 3356.
[3] LD Chiaradia; R dos Santos; CE Victor; AA Vieira; PC Leal; R J Nunes; JB Calixto; R A Yunes*; Bioorg. Med. Chem.*, **2008**, 16, 658.
[4] BP Bandgar; SS Gawande; RG Bodade; NM Gawande; CN Khobragade*; Bioorg. Med. Chem*., **2009**, 17, 8168.
[5] R Li; GL Kenyon; FE Cohen; X Chen; B Gong; JN Dominguez; JE Davidson; G Kurzban; RE Miller; E Nuzum; PJ Rosenthal; JH Mc Kerrowis; *J. Med. Chem*.,**1995**, 38, 5031.
[6] BP Bandgar; SS Gawande; RG Bodade; JV Totre; CN Khobragade*; Bioorg. Med. Chem*., **2010**, 18, 1364.
[7] J Mojzis; L Varinska; G Mojzisova; I Kostova; L Mirossay; *Arch. Pharm. Res.*, **2008**, 57, 259.
[8] D Kumar; NM Kumar; K Akamatsu; E Kusaka; H Harada; T Ito*; Bioorg. Med. Chem. Lett.*, **2010**, 20, 3916.
[9] BJ Gaede; LL Mcdermott; *J. Heterocycl. Chem*., **1993**, 30, 49.
[10] K Shibata; I Katsuyama; H Izoe; M Matsui; H Muramatsu; J. *Heterocycl. Chem.*, **1993**, 30,277.
[11] X Jiaxi; C Wang; Q Zhang; Heteroatom *Chem.*, **2001**, 12, 557.
[12] D Millán; M Domínguez; MC Rezende*; Dyes Pigm.* **2008**, 77,441.
[13] L Mager; C Melzer; M Barzoukas; A Fort; S Mery; JF Nicoud; *Appl. Phys. Lett.*,**1997**,71, 2248.
[14] B Gu; W Ji; PS Patil; SM Dharmaprakash; *J. Appl. Phys.*,**2008**, 103, 511.
[15] AK Singh; G Saxena; R Prasad; A Kumar; *J. Mol. Struct.* , **2012**, 1017, 30.
[16] RW Munn; CN Ironside; *Principles and Applications o f Nonlinear Optical Materials*, Chapman & Hall, London, **1993**, 334.
[17] AI Vogel, *Practical Organic Chemistry*, Pretence Hall Publication, New York, **1956**, 344.
[18] LJ Furrugia; *J. Appl. Cryst*., **1999**, 32, 837-838.
[19] SHELX 97, GM Sheldrick; *Acta Cryst*., **2008**, 112-122.
[20] MN Burnett; C K Jhonson; *ORTEP. III* Oak Ridge, *Thermal Ellipsoid plot, Program for Crystal structure Illustration*, Report ORNL-6895, Oak Ridge National Laboratory, Oak Ridge, TN, USA, **1996**.
[21] AL Spek; *Acta Cryst*. **1999,** 32, 837-838.
[22] Gaussian 09, Revision D.01, MJ Frisch; GW Trucks; H B Schlegel; GE Scuseria et al., Gaussian, Inc., Wallingford CT, **2013**.
[23] K Wolinski; JF Hinton; P Pulay; *J. Am. Chem. Soc*., **1990**, 112, 8251–8260.
[24] P Pulay; G Fogarasi; F Pang; JE Boggs; *J. Am. Chem. Soc*.,**1979**, 101,2550.
[25] JML Martin; V Alsenoy; CV Alsenoy; Gar2ped, University of Antwerp, **1995**.
[26] T Yanai; DP Tew; NC Handy; *Chem. Phys Let.*, **2004**, 393, 51-57.
[27] B Camino; M De-La-Pierre; AM Ferrari; *J. Mol. Struct.*, **2013**, 1046, 116–123.

[28] A Irfan; R Jin; AG Al-Sehemi; AM Asiri; *Spectrochim Acta Part A: Mol. Biom. Spectr.* , **2013**,110, 60-66.
[29] V Barone; M Cossi; J Thomasi; *J.Comput.Chem.* **1998**, 19, 404-417.
[30] M Sarafran; A Komasa; EB Adamska; *J. Mol. Struct*., **2007**, 827,101-107.
[31] Computer program Gauss View 5.0.9, Gaussian Inc, Wallingford, CT 06492 USA.
[32] Todd A Keith; AIM All (Version 10.05.04, Professional) **1997–2010**.
[33] YS Mary; HT Varghese; CY Panicker; T Ertan; I Yildiz; O Temiz-Arpaci; *Spectrochim. Acta*, **2008**, 71A, 566–571.
[34] JA Pople; HB Schlegel; R Krishnan; DJ Defrees; JS Binkley; MJ Frisch; RA Whiteside; RF Hout; WJ Hehre; *Int. J. Quantum Chem.*, **1981**, 15,269–278.
[35] RM Silverstein; F X Webster; *Spectroscopic Identification of Organic Compounds*, Sixth ed., John Wiley & Sons, Inc. New York, **2005**.
[36] P Pulay; G Fogarasi; F Pang; JE Boggs, *J. Am. Chem. Soc*.,**1979**, 101, 2550–2560.
[37] G Socrates; *Infrared and Raman Characteristic Group Frequencies: Tables and Chart*, Wiley, John & Sons, Chichester, New York, **2001**.
[38] N Choudhary; S Bee; A Gupta; P Tondon; *Comp. Theor. Chem.*, **2013**, 1016, 8-21.
[39] J Fleming; *Frontier Orbitals and Organic Chemical Reactions*, 249 s, Wiley, London, **1976**.
[40] SW Xia; X Xu; Y L Sun; Y L Fan; YH Fan; CF Bi; DM Zhang; LR Yang; *Chin. J. Struct. Chem*., **2006**, 25, 849.
[41] K Wolinski; JF Hinton; JF Pulay; *J. Am. Chem. Soc*.,**1990**, 112,8251.
[42] E Scrocco; J Tomasi; *Adv. Quantum. Chem*., **1978**, 11,115-193.
[43] FJ Luque; JM lopez; M Orozco; *Theor. Chem. Acc*., **2000**, 103, 343-345.
[44] E Scrocco; J Tomasi; *Curr. Chem*., **1973**, 7, 95-170.
[45] ED Glendening; AE Reed; JE Carpenter; F Weinhold; NBO Version 3.1,Gaussian Inc. Pittsburgh. PA.
[46] D Geo; L Goodman; *J. Phys. Chem*., **1996**, 100, 12540-12545.
[47] F Weinhold; *Nature*, **2001**, 411, 539-541.
[48] CG Liu; ZM Su; XH Guan; S Muhammad; *J. Phys. Chem.* , **2011**, C 115, 23946–23954.
[49] J Padmanabhan; R Parthasarathi; V Subramaniaan; PK Chattaraj; J. Phys. Chem. , **2007**, A 111,1358.
[50] RG Parr; W Yang; *Density Functional Theory of Atoms and Molecules*, Oxford University Press, Oxford, New York, **1989**.
[51] RG Parr; LV Szentpály; S Liu*; J. Am. Chem. Soc*.,**1999**, 121,1922.
[52] P Geerlings; FD Proft; W Langenaeker; *Chem. Rev*., **2003**,103, 1793.
[53] PK Chattaraj; S Giri; S Duley; *Chem. Rev*., **2011**,111,43-75.
[54] YR Shen; *The Principles of Nonlinear Optics*, Wiley, New York, **1984**.
[55] PV Kolinsky; *Opt. Eng*., **1992**, 31, 1676-11684.
[56] LN Kuleshova; MY Antipin; VN Khrustalev; DV Gusev; ES Bobrikova; *Kristallogra"ya* , **2003**,48,594–601.
[57] AK Singh; G Saxena; R Prasad; A Kumar; *J. Mol. Struct*., **2012**,1017,30.
[58] U Koch; P Popelier; *J. Phys. Chem. Soc*., **1995**, A99.
[59] I Rozas; I Alkorta; J Elguero; *J. Am. Chem. Soc*., **2000**, 122, 11154.
[60] E Espinosa; E Molins; C Lecomte; *Chem. Phys. Lett*., **1998**, 285,170.
[61] M Karabacak; S Bilgli; A Atac; *Spectrochim Acta Part A: Mol. Biom. Spectr.*, **2015**,134,598-607.